Published in final edited form as:
J Biol Inorg Chem. 2012 October ; 17(7): 1071–1082. doi:10.1007/s00775-012-0920-1.

Identification of Cys^{94} as the distal ligand to the Fe(III) heme in the transcriptional regulator RcoM-2 from *Burkholderia xenovorans*

Aaron T. Smith,
Department of Chemistry, University of Wisconsin–Madison, 1101 University Ave., Madison, WI 53706, USA

Katherine A. Marvin,
Department of Chemistry, University of Wisconsin–Madison, 1101 University Ave., Madison, WI 53706, USA

Katherine M. Freeman,
Department of Chemistry, University of Wisconsin–Madison, 1101 University Ave., Madison, WI 53706, USA

Robert L. Kerby,
Department of Bacteriology, University of Wisconsin–Madison, 1550 Linden Drive, Madison, WI 53706, USA

Gary P. Roberts, and
Department of Bacteriology, University of Wisconsin–Madison, 1550 Linden Drive, Madison, WI 53706, USA

Judith N. Burstyn
Department of Chemistry, University of Wisconsin–Madison, 1101 University Ave., Madison, WI 53706, USA

Judith N. Burstyn: burstyn@chem.wisc.edu

Abstract

The CO-responsive transcriptional regulator RcoM from *Burkholderia xenovorans* (BxRcoM) was recently identified as a Cys(thiolate)-ligated heme protein that undergoes a redox-mediated ligand switch; however, the Cys bound to the Fe(III) heme was not identified. To that end, we generated and purified three Cys-to-Ser variants of BxRcoM-2—C94S, C127S, and C130S—and examined their spectroscopic properties in order to identify the native Cys(thiolate) ligand. Electronic absorption, resonance Raman, and electron paramagnetic resonance (EPR) spectroscopies demonstrate that the C127S and C130S variants, like wild-type BxRcoM-2, bind a six-coordinate low-spin Fe(III) heme using a Cys/His ligation motif. In contrast, electronic absorption and resonance Raman spectra of the C94S variant are most consistent with a mixture of five-coordinate high-spin and six-coordinate low-spin Fe(III) heme, neither of which are ligated by a Cys(thiolate) ligand. The EPR spectrum of C94S is dominated by a large, axial high-spin Fe(III) signal, confirming that the native ligation motif is not maintained in this variant. Together, these data reveal that Cys^{94} is the distal Fe(III) heme ligand in BxR-coM-2; by sequence alignment,

Correspondence to: Judith N. Burstyn, burstyn@chem.wisc.edu.

Electronic supplementary material The online version of this article (doi:10.1007/s00775-012-0920-1) contains supplementary material, which is available to authorized users.

Cys^{94} is also implicated as the distal Fe(III) heme ligand in BxRcoM-1, another homologue found in the same organism.

Keywords

Heme; Electron paramagnetic resonance; Resonance Raman spectroscopy; Site-directed mutagenesis; Transcription

Introduction

Small, gaseous diatomic molecules, such as O_2, NO, and CO, are important signaling molecules in biological systems; one method nature employs to sense these gases is interaction of the diatomic molecule with a heme cofactor [1–6]. Dioxygen binding to heme in myoglobin and hemoglobin is a well-known paradigm. Examples of heme-based O_2 sensor proteins, in which the dioxygen-binding heme domain regulates function, include *Rhizobium meliloti* FixL (an O_2-sensing heme protein associated with N_2 fixation gene regulation) [7], *Bacillus subtilis* heme-based aerotactic transducer [8], and *Escherichia coli* direct oxygen sensor (EcDOS) [9]. NO is produced endogenously by nitric oxide synthase; at physiological levels, NO plays a role in both neurotransmission and vascular regulation [10]. Examples of heme-containing NO sensors include the bacterial heme nitric oxide/oxygen binding domain proteins [11], mammalian soluble guanylyl cyclase [12], heme-regulated α-subunit of eukaryotic translational initiation factor 2 kinase (HRI) [13], and the putative NO sensors *Drosophila melanogaster* hormone receptor 51 [14], heme-containing *D. melanogaster* nuclear receptor E75 [15], and *Pseudomonas aeruginosa* dissimilative nitrate respiration regulator [16]. CO is also believed to function as a neurotransmitter in mammals, where it is endogenously produced by heme oxygenase [17]. Examples of CO sensors include mammalian neuronal PAS domain protein 2 (NPAS2) [18] (the PAS domain is a domain structure named for the proteins Period, aryl hydrocarbon receptor nuclear translocator, and Simpleminded) and bacterial *Rhodospirillum rubrum* CooA (RrCooA), a heme-containing CO-sensing transcription factor [19, 20], as well as the putative CO sensors *D. melanogaster* E75 [15] and *D. melanogaster* hormone receptor 51 [14].

Recently, a new prokaryotic transcriptional regulator of CO metabolism (RcoM) was isolated from the aerobic, polychlorinated biphenyl degrading bacterium *Burkholderia xenovorans* (LB400) [21, 22]. Two homologous proteins, *B. xenovorans* RcoM (BxRcoM)-1 and BxRcoM-2, were identified in this bacterium and share 93 % sequence similarity. These proteins contain an N-terminal PAS domain and a C-terminal LytTR domain, a DNA-binding domain from the AlgR/AgrA/LytR family. PAS domains frequently function as sensors of environmental signals through the binding of small molecules and may bind various cofactors [23]. LytTR domains are DNA-binding domains that commonly function within transcriptional regulators and may be found in conjunction with PAS sensor domains [24]. In BxRcoM-1 and BxRcoM-2, the N-terminal PAS domain binds a *b*-type heme cofactor that controls CO-dependent DNA binding (Kerby et al., unpublished).

Studies of BxRcoM-1 and BxRcoM-2 revealed the ligation and oxidation state changes that occur at the RcoM heme. The BxRcoM-1 and BxRcoM-2 homologues were first isolated under aerobic conditions, yet they each contained a six-coordinate Fe(II)CO-bound heme [21]. Aerobic photolysis of the Fe(II)CO species resulted in conversion to a six-coordinate, low-spin Fe(III) heme. Site-directed mutagenesis of BxRcoM-1 identified His^{74} as the proximal ligand, and spectral characterization of Fe(III)BxRcoM-2 definitively demonstrated that the protein bears a cysteine(thiolate) ligand *trans* to a neutral ligand, presumably the same His^{74}. BxRcoM-2 was shown to undergo a redox-mediated ligand

switch in which the cysteine(thiolate) ligand is lost upon heme reduction. The spectral signatures of Fe(II)BxRcoM-2 were consistent with the presence of methionine *trans* to His^{74}; mutagenesis data suggested that the distal Fe(II) ligand for BxR-coM-1, and by analogy BxRcoM-2, is Met^{104} [21, 25]. Methionine, a weaker ligand than histidine, may be more easily replaced by CO; consistent with this understanding, resonance Raman data of the heme–CO adduct in BxR-coM-2 were indicative of CO binding *trans* to the proximal His^{74} [25]. Thus, the proximal ligand His^{74} remains constant during redox- and CO-binding events, whereas the distal ligand is exchanged in order to allosterically modulate BxRcoM DNA-binding behavior to initiate transcription. Although the mutagenesis studies were on BxRcoM-1 and the spectroscopic studies were on BxRcoM-2, the presence of His^{74} and Met^{104} in the N-terminal PAS domains of both proteins implies that the same amino acids are the Fe(II) ligands in these two closely related homologues.

The identity of the cysteine ligand remained in question. Only three cysteine residues are found in the sequences of BxRcoM-1 and BxRcoM-2: Cys^{94}, Cys^{127}, and Cys^{130}. All three cysteine residues were considered as potential Fe(III) ligands, since they all occur within the heme-binding PAS domain. We examined sequences of 16 homologous RcoM proteins to determine the degree of conservation of these three cysteine residues [21]. Cys^{94} and Cys^{127} are not well conserved. Cys^{94} appears in only three proteins, BxRcoM-1, BxRcoM-2, and the RcoM homologue of *Alkalilimnicola ehrlichei*. Cys^{127} appears only twice, in BxRcoM-1 and BxRcoM-2. In contrast, Cys^{130} is moderately conserved, appearing in eight of the 16 RcoM homologues. Thus, amino acid conservation suggests that Cys^{130} is the most likely candidate for the cysteine ligand. Examination of sequences of other *Burkholderia* species revealed evidence for two putative RcoM proteins in *B. cepacia*. Sequence alignments of BxRcoM-1 and BxRcoM-2 with the postulated RcoM proteins from *B. cepacia* strains CH1-1 and BH160 show 88 and 85 % amino acid identity, respectively (Fig. 1). Two of the three cysteines are conserved among all four proteins: Cys^{94} and Cys^{130}. In place of Cys^{127} is Ser^{127} in the *B. cepacia* BH160 sequence, suggesting that Cys^{127} is least likely to be the heme ligand in the BxRcoM proteins. Both Cys^{94} and Cys^{130} are conserved, and are therefore more likely candidates.

Herein, we present identification of Cys^{94} as the cysteine(thiolate) ligand to the Fe(III) heme in BxRcoM-2. Because there were only three cysteines, we chose to isolate variants in which each of the three was altered; surprisingly, the evidence unequivocally identifies Cys^{94} as the thiolate ligand. Spectroscopic signatures of the three BxRcoM-2 variants—C94S, C127S, and C130S—were studied using electronic absorption, resonance Raman, and electron paramagnetic resonance (EPR) spectroscopies. The Fe(III) C94S variant exhibits differences in its spectroscopic features from those of wild-type Fe(III)BxRcoM-2 and the other variants, and the spectral signatures of Fe(III) C94S are inconsistent with coordination of a cysteine(thiolate) ligand to the Fe(III) heme.

Materials and methods

Materials

Glycerol (greater than 99.5 % purity) and all chemicals used in buffer preparation (99.5 % purity or better) were purchased from Sigma-Aldrich and used as received. Certified ACS grade potassium ferricyanide—$K_3[Fe(CN)_6]$—was purchased from Sigma-Aldrich and used as received. Sodium dithionite ($Na_2S_2O_4$; 85 % purity) was purchased from Fluka and stored under argon gas at 253 K until it was used. A CO gas (99.5 % purity) cylinder was obtained from AGA.

Mutagenesis, isolation, and purification of BxRcoM-2 variants

Variant proteins were generated by mutagenesis of the cloned BxRcoM-2 [21] according to the QuikChange protocol [Agilent Technologies (Stratagene), Santa Clara, CA, USA]. Sequences of all constructs were verified with BigDye v. 3.1 reaction chemistry [Life Technologies (Applied Biosystems), Carlsbad, CA, USA] and subsequent analysis by the University of Wisconsin–Madison Biotechnology Center DNA sequencing facility.

Isolation and purification of the BxRcoM-2 variants was similar to that described in our previous reports [21, 25]. Briefly, *E. coli* VJS6737 [26] bearing the pEXT20 expression vector [27] for the appropriate variant was cultivated in rich medium supplemented with ferric citrate. Isopropyl β-D-thiogalactopyranoside (7 μM) was used to induce expression for 18–20 h at 301 K. Cells were pelleted by centrifugation (10,000*g*, 10 min), resuspended in lysis buffer [50 mM 3-(*N*-morpholino)propanesulfonic acid (MOPS), pH 7.5, 500 mM KCl, and 0.5 mM dithio-threitol], and lysed by passage through a French press. A nickel nitriloacetic acid column (Qiagen, 8-mL resin volume) was preequilibrated with 10 mM imidazole, 50 mM MOPS, pH 7.5, 500 mM KCl. The cell supernatant (25 mL) was applied slowly, and the column was washed successively with 10 mM imidazole (two column volumes) and 50 mM imidazole (one column volume), in the same buffer. Finally, protein was eluted with 220 mM imidazole. The protein was precipitated at 55 %-saturated $(NH_4)_2SO_4$ (v/v) with incubation on ice for 30 min and brief centrifugation. The protein pellet was dissolved in 500 μL 25 mM MOPS, pH 7.4 and 500 mM KCl, applied to a buffer-equilibrated Sephadex G-25 column, and eluted in the same buffer. The desalted protein was stored at 193 K. Protein concentrations were determined using the bi-cinchoninic acid method (Pierce, Rockford, IL, USA); sodium dodecyl sulfate polyacrylamide gel electrophoresis verified protein purity was greater than 90 %; heme content was determined using the pyridine hemochromogen assay [28].

Electronic absorption spectroscopy

Electronic absorption spectra were recorded with a double-beam Varian Cary 4 Bio spectrophotometer set to a spectral bandwidth of 0.5 nm. Spectra were acquired at room temperature for samples of protein prepared, as indicated in the figure legends, in either 25 mM MOPS buffer, pH 7.4, or 25 mM 3-[4-(2-hydroxyethyl)-1-piperazinyl]propane-sulfonic acid (EPPS) buffer, pH 8.0, with 500 mM KCl. Oxygen was removed from anaerobic samples by flowing argon gas through the headspace of a septum-sealed cuvette for at least 10 min. Reduction of Fe(III) protein samples was accomplished either by adding an anaerobically prepared stock solution of sodium dithionite to achieve a final sample concentration of 1–5 mM or by adding a few solid crystals of sodium dithionite to the protein sample solution with argon gas flowing in the cuvette headspace. The Fe(II)CO adducts were prepared by the injection of CO via a gastight syringe into the headspace of a septum-sealed cuvette containing the Fe(III) or as-isolated protein, followed by gentle agitation of the sample and addition of the dithionite reductant. Final protein and heme concentrations ranged from 7 to 10 μM, and 100–200 μL of CO gas was injected, as appropriate, to give complete conversion to the Fe(II)CO adduct.

Reoxidation of the Fe(II)BxRcoM-2 variants

Protein that was present in the Fe(II) state to a significant extent after purification was reoxidized using potassium ferricyanide. A stock solution of potassium ferricyanide (500 μL, 25 mM) was prepared by dissolving 4–5 mg of solid potassium ferricyanide in 500 μL of 25 mM MOPS, pH 7.4, with 500 mM KCl. This stock solution was added to the protein sample to a final concentration of 1–2 mM. The mixture was allowed to react for 20–30 min. The protein solution was loaded onto a YM-30 Amicon Ultra spin concentrator (Millipore) and washed four times by concentration and dilution into fresh MOPS buffer (25 mM pH

7.4, 500 mM KCl) using a tabletop centrifuge (relative centrifugal force 15,000*g*) to remove excess potassium ferricyanide. Final heme and protein concentrations were determined using the pyridine hemochromogen assay [28] and the bicinchoninic acid assay (Pierce, Rockford, IL, USA), respectively.

EPR spectroscopy

X-band EPR spectra were collected with a Bruker ELEX-SYS E500 instrument equipped with an Oxford Instruments ESR 900 continuous-flow liquid helium cryostat and an Oxford Instruments ITC4 temperature controller maintained at 10 K. The microwave frequency was monitored using an EIP model 625A continuous-wave microwave frequency counter. Protein samples were prepared, as indicated in the figure legends, in either 50 mM borate, pH 8.0, or 25 mM MOPS, pH 7.4, with 500 mM KCl. Samples were transferred to a quartz EPR tube via small-bore tubing (connected to a gastight syringe) and frozen in liquid nitrogen. Samples of approximately 150 μL had a final concentration of 80–250 μM heme. For all samples, scans from 0 to 10,000 G revealed no signals other than those reported.

Resonance Raman spectroscopy

Resonance Raman spectra were obtained with an excitation wavelength of 413.1 nm from a Coherent I-302C Kr^+ laser. Low incident laser powers of less than 20 mW were focused with a cylindrical lens onto the sample. The frozen protein samples, prepared as described for EPR spectroscopy (vide supra), were placed in a quartz dewar and maintained at 77 K in liquid nitrogen to reduce local heating. Light was scattered in an approximately 135° geometry (relative to the sample) and dispersed by an Acton Research triple monochromator with gratings of 2,400 grooves per millimeter. Scattered light was detected using a liquid-nitrogen-cooled CCD camera (Princeton Instruments) under computer control using the Spectra-Sense software package. Peak positions were calibrated relative to the ice peak at 228 cm^{-1} or a Na_2SO_4 peak at 981 cm^{-1}. Windows centered at 650, 1,250, and 1,850 cm^{-1} were overlaid for a total frequency range of 150–2,250 cm^{-1}. IGOR Pro version 6.0 (Wavemetrics) was used to import and process all spectral data. Spectral deconvolutions were achieved using IGOR Pro version 6.0. Peaks were generated by direct combination of a series of Gaussian curves; the amplitudes and frequencies of the Gaussian curves were manually adjusted until the residuals between the native peak and the fitted peak were minimized. Major vibrational modes were assigned on the basis of comparison with those of other heme proteins and the work of Kitagawa and Spiro [29–33].

Results

Characterization of C127S and C130S BxRcoM-2

The electronic absorption spectra of purified C127S and C130S BxRcoM-2 are most consistent with a low-spin, six-coordinate Fe(III) heme ligated by a cysteine(thiolate) and a neutral ligand, presumably His^{74} as in wild-type BxR-coM. Thiolate to low-spin Fe(III) charge transfer gives rise to an intense δ band and two low-energy ligand-to-metal charge transfer (LMCT) transitions, and these characteristic features are present in the electronic absorption spectra of C127S and C130S. The spectrum for C127S (Fig. 2, spectrum c) displays a well-resolved δ band at 354 nm, a sharp, intense Soret (γ) peak at 422 nm, a broad, asymmetric absorption envelope consisting of α and β bands at 562 and 537 nm, respectively, and a pair of weak LMCT transition bands at 648 and 728 nm. Peak positions for C130S are similar (Fig. 2, spectrum b). The electronic absorption spectra of these variants differ only marginally from those of the wild type, suggesting that the heme environments are similar (Table 1, Fig. 2). Reduction (via addition of sodium dithionite) and CO binding to either C127S and C130S results in spectral changes nearly identical to those

observed in wild-type BxRcoM-2 (Figs. S1, S2, Table 1), suggesting that the reduction and CO binding behaviors of these variants are also similar to those of the wild type.

Comparison of the resonance Raman spectra of C127S and C130S with the spectrum of wild-type Fe(III)BxRcoM-2 (Fig. 3) supports the presence of a low-spin, six-coordinate Fe(III) heme with a cysteine(thiolate) ligand in each variant. Porphyrin stretches in the mid-frequency region (1,300–1,700 cm^{-1}) are sensitive to the oxidation state of the heme iron (ν_4), its spin state, and coordination number (ν_3, ν_2, ν_{10}) [31, 32]. Assignments for these bands in wild-type Fe(III)BxRcoM-2 were reported previously [25], and the high-frequency spectrum of the C127S variant bears a striking resemblance to that of the wild type (Fig. 3, spectra a and c, respectively). Similarly, the spectrum of the as-isolated C130S protein overlaps closely with that of wild-type Fe(III)BxRcoM-2 (Fig. S3, spectra b and a, respectively); however, additional bands indicate there is a mixture of Fe(III) and Fe(II) in the as-isolated sample. The spectrum of C130S oxidized with potassium ferricyanide (Fig. 3, spectrum b) is almost identical to that of wild-type Fe(III)BxRcoM-2, and is most consistent with a six-coordinate, low-spin Fe(III) heme; a shoulder persists in the oxidation-state marker band, ν_4, indicative of residual Fe(II) even after oxidation. On the basis of comparisons with resonance Raman spectra of other cysteine(thiolate)-ligated hemoproteins [34–36], an iron–sulfur stretching mode, $\nu_{Fe–S}$, was tentatively identified in the low-frequency region of the wild-type Fe(III)BxRcoM-2 resonance Raman spectrum at 310 cm^{-1} [25]. A similar, broad $\nu_{Fe–S}$ band is observed at 308 cm^{-1} for C127S (Fig. 4, spectrum c) and at 309 cm^{-1} for C130S (Fig. 4, spectrum b).

EPR spectroscopy is also indicative of a low-spin, six-coordinate Fe(III) ($S = 1/2$) heme with a cysteine(thiolate) *trans* to a second, neutral ligand in both C127S and C130S. The EPR spectrum of Fe(III) C127S (Fig. 5, spectrum c) displays a characteristic rhombic signal with g values of 1.91, 2.27, and 2.44, corresponding to g_x, g_y, and g_z, respectively. Similarly, the rhombic EPR signal of Fe(III) C130S (Fig. 5, spectrum b) exhibits g values of 1.88, 2.27, and 2.50. For each variant, the g values are comparable to those obtained for wild-type Fe(III)BxRcoM-2 (Table 2, *g*Fig. 5, spectrum a). Slightly more basic pH and altered buffer conditions may account for differences in the observed values among the variants and wild-type BxRcoM-2. A second minor EPR signal with an axial g anisotropy ($g_\perp = 5.8$) is also observed for the variants C127S and C130S (both as-isolated and reoxidized). This signal is due to a small amount of high-spin Fe(III) heme present, consistent with resonance Raman spectra where a small five-coordinate high-spin band is observed at approximately 1,490 cm^{-1} (ν_3) for both variants (Fig. 3). Taken together, the electronic absorption, resonance Raman, and EPR data for the Fe(III) C127S and Fe(III) C130S variants affirm the native histidine/cysteine(thiolate) ligation motif is maintained.

Characterization of C94S BxRcoM-2

Electronic absorption spectroscopy of purified C94S is strongly suggestive that Cys^{94} is the Fe(III) heme ligand in wild-type BxRcoM-2. Unlike the C127S or C130S variants, the electronic absorption spectra of C94S are most similar to those of Fe(III) hemes lacking a cysteine(thiolate) ligand (Table 1, Fig. 2, spectra d, e). The Soret band at 418 nm of as-isolated C94S is broader than that of wild-type BxRcoM-2, and the α/β bands at 561 and 532 nm, respectively, are more well defined than those expected for a six-coordinate, low-spin Fe(III) heme with cysteine/histidine axial ligands. The pronounced, characteristic δ band of thiolate ligation is absent; in its place is a weak Soret shoulder near 360 nm. Only one LMCT band is observed, at 640 nm, again suggesting that thiolate ligation is absent. Like the C130S variant, resonance Raman analyses initially indicated that C94S was purified as a mixture of the Fe(II) and Fe(III) oxidation states. In contrast to the C130S variant, however, only a weak EPR signal was initially detected (vide infra). Unlike the C130S variant, oxidation of the C94S variant by potassium ferricyanide resulted in a 3-nm

blueshift of the Soret band to 415 nm, a slight decrease in the intensity of the δ band shoulder, and slight shifts in the α/β band positions to 562 and 530 nm, respectively. Additionally, a band at 632 nm appeared, suggesting that a high-spin Fe(III) heme was formed [37]. The observed electronic absorption spectral features are most similar to those of proteins with a mixture of high-spin and low-spin Fe(III) hemes and without a cysteine(thiolate) ligand, such as metmyoglobin, *Acetobacter xylinum* phosphodiesterase A1 (AxPDEA1), and *Methanobacterium thermoautotrophicum* direct oxygen sensor (MtDOS) [37, 38]. The electronic absorption spectra of Fe(II) and Fe(II)CO C94S are virtually identical to those of wild-type BxRcoM (Table 1, Figs. S1, S2), suggesting that the reduction and CO binding behaviors of the C94S variant are unperturbed.

The resonance Raman spectrum for as-isolated C94S (Fig. S3, spectrum d) displays oxidation-state and spin-state marker bands consistent with a mixture of oxidation states, similar to those of the C130S variant. Addition of potassium ferricyanide to as-isolated C94S results in a sharpening of the oxidation-state marker band, with one major frequency exhibited at 1,371 cm^{-1} (Fig. 3, spectrum d), indicative of Fe(III) as the major heme iron oxidation state. A ν_3 shoulder, likely due to residual Fe(II), persisted in all of the samples studied. The high-frequency region that contains the spin and coordination-state marker bands (ν_3 and ν_2) displays broadened bands at 1,493 and 1,503 cm^{-1} (ν_3) and 1,562 and 1,577 cm^{-1}(ν_2). These band positions are indicative of a mixture of low-spin and high-spin Fe(III) hemes, which is most similar to what is observed in the met forms of Fe(III)AxPDEA1 and Fe(III)MtDOS [38]. In addition, the spin-state marker band ν_{10} is not observed in the resonance Raman spectrum of C94S, unlike the ν_{10} band of the Fe(III) forms of wild-type, C130S, and C127S BxRcoM-2. Presumably, ν_{10} in C94S is shifted to lower energy and is hidden owing to overlap with the strong, Gaussian-shaped $\nu_{c=c}$ band at 1,622 cm^{-1}.

Distinct differences in the low-frequency region of the resonance Raman spectrum of C94S support the conclusion that Cys^{94} is the native cysteine ligand. In the region where $\nu_{Fe–S}$ is typically seen, there is a band at 304 cm^{-1} that is sharpened and downshifted relative to the comparable band of wild-type BxRcoM-2 (Fig. 4). This 304-cm^{-1} mode might plausibly be attributed to an Fe–S(thioether) stretch, since Met^{104} is the distal Fe(II) ligand; however, we believe that this mode is actually a porphyrin vibration. Gaussian deconvolution of the broad $\nu_{Fe–S}$ bands of Fe(III) wild-type, C130S, and C127S BxRcoM-2 (Fig. 4) generated best fits with three overlapping components. For the C94S spectrum, a single Gaussian was sufficient to fit the sharp band at 304 cm^{-1}. Because the 304-cm^{-1} component peak is present in the low-energy resonance Raman region of wild-type BxRcoM-2 and all the variants, we assign this band to a porphyrin mode. We attribute the two higher-energy components (313 and 321 cm^{-1}) of Fe(III) wild-type, C130S, and C127S BxRcoM-2 to $\nu_{Fe–S}$. These $\nu_{Fe–S}$ bands overlap with the porphyrin mode centered at 304 cm^{-1}, like that of cysteine-ligated NPAS2 [39]. A new, intense band at 226 cm^{-1} is seen in the resonance Raman spectrum of C94S reacted with potassium ferricyanide, which we tentatively assign as the $\nu_{Fe–His}$ stretch of the proximal ligand His^{74}. The rationale for this assignment is the large resonance enhancement of the $\nu_{Fe–His}$ stretch, which typically appears in the 220–270-cm^{-1} region. This intense feature is typically observed in five- and six-coordinate ferrous hemoproteins with an axial histidine ligand, such as oxymyoglobin, oxyhemoglobin, deoxyhemoglobin, microperoxidase, *Bradyrhizobium japonicum* FixL, and MtDOS [38, 40–42]. A similarly intense Fe–His stretch is observed in five-coordinate ferric metmyoglobin [43].

EPR characterization of C94S provides confirmation that Cys^{94} is the sixth ligand to the Fe(III) heme in wild-type BxRcoM-2. Data collected for the as-isolated C94S revealed no distinct set of rhombic signals between 2,400 and 3,800 G; however, a low-intensity axial

signal at $g_{\perp}$ = 5.8 was observed, consistent with a high-spin Fe(III) heme. Addition of ferricyanide to the as-isolated form of C94S resulted in an increase in intensity (Fig. 5, spectrum d) of this high-spin axial signal with $g_{\perp}$ = 5.82 and $g_{\|}$ = 2.00. This axial spectrum is typical of high-spin hemoproteins such as aquo metmyoglobin and high-spin cytochrome *c* oxidase [44, 45]. The EPR spectrum of the C94S protein (Fig. 5, spectrum d) also contains a small rhombic signal that we attribute to the fraction of low-spin Fe(III). The *g* anisotropy of this low-spin signal is comparable to that of wild-type BxRcoM, C127S, and C130S, suggesting that Cys^{127} or Cys^{130} may replace Cys^{94} in a fraction of the C94S protein. The fact that the EPR spectrum of C94S exhibits predominantly high-spin Fe(III), and not low-spin Fe(III) like that of wild-type BxRcoM-2, is clear evidence that the cysteine ligand has been lost in this variant. Taken together, our spectral data implicate Cys^{94} as the distal Fe(III) heme ligand in BxRcoM-2.

Discussion

Numerous heme proteins are implicated in sensing and transport of small molecules [1, 4, 6]; discrimination among the gaseous signal transducers O_2, NO, and CO requires a recognition mechanism that is not based on charge, shape, or size because these gases cannot be readily differentiated by these methods. Instead, heme proteins must modify their affinity for small molecules by altering the iron redox potential, oxidation state, spin state, distal or proximal ligands, or interactions of the gas molecule with residues in the heme-binding pocket [2]. Functional activity of gas-sensing heme proteins is frequently linked to the nature of the heme-binding environment. One element of control utilized to poise the heme for gas binding is a redox-mediated ligand switch; however, the discriminatory binding of gas molecules is modulated by a combination of factors that a redox-mediated ligand switch alone cannot confer. In many cases, a series of events occurs in which the heme iron atom changes oxidation and ligation states preceding gas binding; the final step of regulation is commonly achieved upon stabilization of the correct effector molecule in the heme-binding pocket.

In EcDOS, binding of O_2 to heme regulates phosphodiesterase activity [3, 46]. The EcDOS Fe(III) heme, bound within a PAS domain, is coordinated by a histidine residue (His^{77}) and an exogenous water molecule [47]. Reduction of Fe(III) heme to Fe(II) heme results in replacement of the coordinated water by a methionine (Met^{95}) as the distal heme ligand [48, 49]. O_2 binding to Fe(II)EcDOS proceeds via replacement of the weakly bound Met^{95} thioether group. Structural and spectroscopic studies have revealed that charge buildup on the coordinated O_2, which does not happen upon CO or NO binding, is neutralized via the guanidinium group of Arg^{97} [47, 49, 50]. The environment of the heme-binding pocket in EcDOS enables the protein to enhance selectivity for O_2 over CO or NO and prevents autoxidation of the heme iron upon O_2 binding [3, 50, 51].

HRI, which regulates globin synthesis in reticulocytes in response to available heme levels, is a multidomain heme protein with two distinct heme-binding sites, one of which is a low-spin, six-coordinate heme–thiolate center that functions as an NO sensor [52, 53]. Cys^{409} of the kinase domain and a histidine (His^{119} or His^{120}) of the N-terminal domain serve as ligands to this NO-binding heme. Characteristics of cysteine(thiolate) coordination are lost following reduction, suggesting that either a ligand switch or protonation to a cysteine(thiol) occurs to stabilize the more-electron-rich Fe(II) heme [54, 55]. HRI activity is specifically upregulated by formation of a five-coordinate NO adduct, which occurs owing to the strong *trans* influence of NO and the weakly coordinating nature of the histidine ligand. CO binding opposite the anchoring histidine, forming a six-coordinate species, suppresses activity in HRI, and reaction with O_2 results in autoxidation [53]. It is postulated that NO

binding releases inhibition by the HRI heme domain, whereas binding of other gas-signaling molecules does not [56].

RrCooA is the first-known and best-characterized CO gas sensor. This homodimeric protein binds a heme *b* cofactor within each monomer and utilizes heme-dependent control to regulate expression of genes encoding CO-metabolizing enzymes [20, 57, 58]. The Fe(III) heme in RrCooA is low-spin and six-coordinate; the axial ligands to the Fe(III) heme are a cysteine(thiolate) (Cys^{75}) and the N-terminal proline (Pro^{2}) from the other monomer of the dimer [59–61]. Reduction of the heme iron results in replacement of the cysteine(thiolate) ligand (Cys^{75}) with histidine (His^{77}) [61, 62]. RrCooA is unusual in that the weakly coordinated N-terminal proline (Pro^{2}) is retained during the redox exchange and thereafter is replaced by the exogenous CO molecule [60, 63]. Binding of CO initiates conformational changes that are propagated along the dimer interface, ultimately resulting in DNA binding [60, 63–66]. Addition of O_2 to Fe(II)RrCooA results in autoxidation, which causes the protein to revert to the Cys–His axial coordination characteristic of the Fe(III) heme [20]. NO reacts with either Fe(III) or Fe(II)RrCooA to form a five-coordinate Fe(II)–NO heme, which is inactive toward DNA binding [67]. Thus, RrCooA is also able to discriminate between O_2, CO, and NO, and regulate the biological response of *R. rubrum* to its environment.

In a manner similar to RrCooA, the isolated PAS-A domain of the mammalian CO sensor NPAS2 bears an Fe(III) heme that is low-spin and is ligated by a histidine/cysteine(thiolate) motif. Upon reduction of the Fe(III) heme, the cysteine(thiolate) ligand (Cys^{170}) is replaced with a strong donor, postulated to be the deprotonated side chain of His^{171} [39]. One of the histidines is then released to bind CO: whether this is His^{119} or His^{171} is not clear. CO-dependent signaling is transduced through the PAS-A domain via disruption of a hydrogen-bonding network, which ultimately causes dissociation of NPAS2 from its heterodimeric partner brain and muscle Arnt-like protein 1 (BMAL1). Dissociation of the DNA-binding NPAS2–BMAL1 complex prevents transcription of *per* and *cry* genes, both of which are involved in regulation of the circadian clock [18, 39, 68]. NPAS2 is reported neither to bind O_2 reversibly nor to interact with NO [18]. The structural basis for this discrimination is unknown, but it is hypothesized that secondary interactions in the heme-binding pocket contribute.

Recent spectroscopic studies and in vivo functional assays have linked the heme-containing BxRcoM proteins to aerobic CO sensing [21, 25]. Similar to other small-molecule sensor proteins that respond to O_2, CO, and NO binding, BxRcoM function is modulated by the oxidation state of the heme iron and by the ligand environment of the heme cofactor. Our prior studies demonstrated that BxR-coM-2 is a cysteine-ligated heme protein that undergoes a redox-mediated ligand switch [25]. In the Fe(III) state, the proximal ligand is inferred to be His^{74} on the basis of sequence similarity to and site-directed mutagenesis studies of the homologous BxRcoM-1 protein (vide supra) [21]. The BxRcoM-1 and BxRcoM-2 proteins contain three cysteine residues as the potential distal ligand to the Fe(III) heme: Cys^{94}, Cys^{127}, and Cys^{130}. Given the involvement of cysteine(thiolate) residues in redox-mediated ligand switches, which appear to prime gas-regulated hemoproteins for effector-mediated response, we set out to identify the Fe(III)BxRcoM cysteine(thiolate) ligand.

Herein, Cys^{94} was identified as the distal Fe(III) heme ligand in BxRcoM-2. Sequence alignments of putative RcoM homologues suggested Cys^{130} was the likelier heme ligand candidate. Three cysteine-to-serine variants were generated, and unlike the other variants studied, the spectral data strongly suggest that C94S does not possess the native low-spin Fe(III) heme with histidine/cysteine(thiolate) coordination. The EPR spectrum of C94S was

dominated by an axial signal characteristic of high-spin heme, providing the most compelling evidence that the strongly donating thiolate axial ligand was absent. A minor low-spin component was also observed, suggesting that a sixth ligand may bind in place of Cys^{94} in a small population of the Fe(III) C94S variant. Given the apparent *g* anisotropy of this weak low-spin signal, we speculate that Cys^{130}, the most conserved of the three cysteines, or possibly Cys^{127}, may replace the native Cys^{94}. The electronic absorption spectrum of C94S lacked the well-resolved δ band and the two weak LMCT bands in the visible region characteristic of a low-spin thiolate-ligated heme. Furthermore, resonance Raman data suggested that the Fe–S stretch was absent, and a new band at 226 cm^{-1} was tentatively assigned as a $\nu_{Fe–His}$ mode of a high-spin heme. Thus, all the spectral data point to Cys^{94} as the heme ligand in BxRcoM-2 although this residue is not highly conserved among RcoM proteins. It remains to be seen whether other RcoM proteins bear heme, whether they employ cysteine coordination, or whether Cys^{130} plays some other role in signal transduction in these proteins.

In combination with our past results on the BxRcoM proteins, these data illustrate a mechanism by which the BxRcoM proteins utilize changes in oxidation and ligation states at the heme cofactor to poise the protein to respond to CO (Scheme 1). BxRcoM proteins are members of a family of cysteine(thiolate)-coordinated heme proteins that undergo redox-mediated ligand exchange and selective ligand replacement as components of the machinery to affect protein function. As shown in Scheme 1, reduction of the low-spin, six-coordinate Fe(III) heme center in BxRcoM results in the loss of the cysteine(thiolate) distal ligand; this ligand is now known to be Cys^{94}. Loss of a cysteine(thiolate) ligand from a low-spin six-coordinate heme serves as a priming reaction that prepares BxRcoM to respond to its effector molecule, similar to what is observed in RrCooA and NPAS2. BxRcoM Cys^{94} is replaced by a neutral, weakly bound ligand, presumably Met^{104}; Met^{104} is then replaced by CO. Met^{104} serves an analogous function to Met^{95} in the heme–PAS O_2 sensor EcDOS [47, 69], as the more weakly bound, more readily replaced ligand in a low-spin six-coordinate heme complex. Thus, the BxRcoM proteins utilize a hybrid of the strategies seen in RrCooA, NPAS2, and EcDOS to ready themselves for gas-dependent transcriptional activation. Ultimately, the redox-mediated ligand switch from Cys^{94} [Fe(III)] to Met^{104} [Fe(II)] is crucial to maintaining the sensitivity of the BxRcoM proteins to CO; however, the exact discriminatory nature of the RcoM proteins for CO over O_2 and NO and the mode of propagation of this signal to the LytTR DNA-binding domain are still unknown.

Supplementary Material

Refer to Web version on PubMed Central for supplementary material.

Acknowledgments

The authors thank Thomas C. Brunold (University of Wisconsin–Madison) and his research group for their expertise and the generous use of their instrumentation. Rapid DNA sequencing procedures were performed at the University of Wisconsin–Madison Biotechnology Center facility. Sequence searches utilized both database and analysis functions of the Universal Protein Resource (UniProt) Knowledgebase and Reference Clusters (http://www.uniprot.org) and the National Center for Biotechnology Information (http://www.ncbi.nlm.nih.gov/). This work was supported by NIH grant GM-53228 to G.P.R. and HL-065217 to J.N.B.

Abbreviations

AxPDEA1	*Acetobacter xylinum* phosphodiesterase A1
BMAL1	Brain and muscle Arnt-like protein 1
BxRcoM	*Burkholderia xenovorans* regulator of CO metabolism

EcDOS	*Escherichia coli* direct oxygen sensor
EPR	Electron paramagnetic resonance
HRI	Heme-regulated α-subunit of eukaryotic translational initiation factor 2 kinase
LMCT	Ligand-to-metal charge transfer
MOPS	3-(*N*-Morpholino)propanesulfonic acid
MtDOS	*Methanobacterium thermoautotrophicum* direct oxygen sensor
NPAS2	Neuronal PAS domain protein 2
RcoM	Regulator of CO metabolism
RrCooA	*Rhodospirillum rubrum* CooA

References

1. Uchida T, Kitagawa T. Acc Chem Res. 2005; 38:662–670. [PubMed: 16104689]
2. Jain R, Chan MK. J Biol Inorg Chem. 2003; 8:1–11. [PubMed: 12459893]
3. Sasakura Y, Suzuki-Yoshimura T, Kurokawa H, Shimizu T. Acc Chem Res. 2006; 39:37–43. [PubMed: 16411738]
4. Aono, S. Dalton Trans. 2008. p. 3137-3146.
5. Spiro S. Biochem Soc Trans. 2008; 36:1160–1164. [PubMed: 19021516]
6. Gilles-Gonzalez M-A, Gonzalez G. J Inorg Biochem. 2005; 99:1–22. [PubMed: 15598487]
7. Gilles-Gonzalez MA, Ditta GS, Helinski DR. Nature. 1991; 350:170–172. [PubMed: 1848683]
8. Hou S, Larsen RW, Boudko D, Riley CW, Karatan E, Zimmer M, Ordal GW, Alam M. Nature. 2000; 403:540–544. [PubMed: 10676961]
9. Delgado-Nixon VM, Gonzalez G, Gilles-Gonzalez M-A. Biochemistry. 2000; 39:2685–2691. [PubMed: 10704219]
10. Ignarro LJ. Angew Chem Int Ed. 1999; 38:1882–1892.
11. Karow DS, Pan D, Tran R, Pellicena P, Presley A, Mathies RA, Marletta MA. Biochemistry. 2004; 43:10203–10211. [PubMed: 15287748]
12. Ignarro LJ, Degnan JN, Baricos WH, Kadowitz PJ, Wolin MS. Biochim Biophys Acta. 1982; 718:49–59. [PubMed: 6128034]
13. Igarashi J, Sato A, Kitagawa T, Yoshimura T, Yamauchi S, Sagami I, Shimizu T. J Biol Chem. 2004; 279:15752–15762. [PubMed: 14752110]
14. de Rosny E, de Groot A, Jullian-Binard C, Borel F, Suarez C, Le Pape L, Fontecilla-Camps JC, Jouve HM. Biochemistry. 2008; 47:13252–13260. [PubMed: 19086271]
15. Reinking J, Lam MMS, Pardee K, Sampson HM, Liu S, Yang P, Williams S, White W, Lajoie G, Edwards A, Krause HM. Cell. 2005; 122:195–207. [PubMed: 16051145]
16. Giardina G, Rinaldo S, Johnson KA, Di Matteo A, Brunori M, Cutruzzola F. J Mol Biol. 2008; 378:1002–1015. [PubMed: 18420222]
17. Verma A, Hirsch DJ, Glatt CE, Ronnet GV, Snyder SH. Science. 1993; 259:381–384. [PubMed: 7678352]
18. Dioum EM, Rutter J, Tuckerman JR, Gonzalez G, Gilles-Gonzalex M-A, Mcknight SL. Science. 2002; 298:2385–2387. [PubMed: 12446832]
19. Aono S, Nakajima H, Saito K, Okada M. Biochem Biophys Res Commun. 1996; 228:752–756. [PubMed: 8941349]
20. Shelver D, Kerby RL, He Y, Roberts GP. Proc Natl Acad Sci USA. 1997; 94:11216–11220. [PubMed: 9326589]
21. Kerby RL, Youn H, Roberts GP. J Bacteriol. 2008; 190:3336–3343. [PubMed: 18326575]

22. Chain PSG, Denef VJ, Konstantinidis KT, Vergez LM, Agulló L, Reyes VL, Hauser L, Córdova M, Gómez L, González M, Land M, Lao V, Larimer F, LiPuma JJ, Mahenthiralingam E, Malfatti SA, Marx CJ, Parnell JJ, Ramette A, Richardson P, Seeger M, Smith D, Spilker T, Sul WJ, Tsoi TV, Ulrich LE, Zhulin IB, Tiedje JM. Proc Natl Acad Sci USA. 2006; 103:15280–15287. [PubMed: 17030797]
23. Gu Y-Z, Hogenesch JB, Bradfield CA. Annu Rev Physiol. 2000; 40:519–561.
24. Nikolskaya AN, Galperin MY. Nucleic Acids Res. 2002; 30:2453–2459. [PubMed: 12034833]
25. Marvin KA, Kerby RL, Youn H, Roberts GP, Burstyn JN. Biochemistry. 2008; 47:9016–9028. [PubMed: 18672900]
26. Stewart V, Lu Y, Darwin AJ. J Bacteriol. 2002; 184:1314–1323. [PubMed: 11844760]
27. Dykxhoorn DM, St Pierre R, Linn T. Gene. 1996; 177:133–136. [PubMed: 8921858]
28. Antonini, E.; Brunori, M. Hemoglobin and myoglobin in their reactions with ligands. North-Holland; Amsterdam: 1971.
29. Abe M, Kitagawa T, Kyogoku Y. J Chem Phys. 1978; 69:4526–4532.
30. Woodruff WH, Adams DH, Spiro TG, Yonetani T. J Am Chem Soc. 1975; 97:1695–1698. [PubMed: 1133400]
31. Spiro TG. Biochim Biophys Acta. 1975; 416:169–189. [PubMed: 169917]
32. Spiro TG, Strekas TC. J Am Chem Soc. 1974; 96:338–345. [PubMed: 4361043]
33. Kitagawa T, Kyogoku Y, Iizuka T, Ikeda-Saito M, Yamanaka T. J Biochem. 1975; 78:719–728. [PubMed: 2584]
34. Champion PM, Stallard BR, Wagner GC, Gunsalus IC. J Am Chem Soc. 1982; 104:5469–5472.
35. Green EL, Taoka S, Banerjee R, Loehr TM. Biochemistry. 2000; 40:459–463. [PubMed: 11148040]
36. Liu Y, Loccoz-Moënne P, Hildebrand DP, Wilks A, Loehr TM, Mauk AG, de Montellano PRO. Biochemistry. 1999; 38:3733–3743. [PubMed: 10090762]
37. Falk, JE. Porphyrins and metalloporphyrins: their general, physical, and coordination chemistry, and laboratory methods. Elsevier; Amsterdam: 1964.
38. Tomita T, Gonzalez G, Chang AL, Ikeda-Saito M, Gilles-Gonzalex M-A. Biochemistry. 2002; 41:4819–4826. [PubMed: 11939776]
39. Uchida T, Sato E, Sato A, Sagami I, Shimizu T, Kitagawa T. J Biol Chem. 2005; 280:21358–21368. [PubMed: 15797872]
40. Kerr EA, Yu N-T, Gersonde K, Parish DW, Smith KM. J Biol Chem. 1985; 260:12665–12669. [PubMed: 4044602]
41. Walters MA, Spiro TG. Biochemistry. 1982; 21:6989–6995. [PubMed: 7159577]
42. Othman S, Lirzin AL, Desbois A. Biochemistry. 1994; 33:15437–15448. [PubMed: 7803408]
43. Hirota S, Mizoguchi Y, Yamauchi O, Kitagawa T. J Biol Inorg Chem. 2002; 7:217–221. [PubMed: 11862557]
44. Peisach J, Blumberg WE, Ogawa S, Rachmilewitz EA, Oltzik R. J Biol Chem. 1971; 246:3342–3355. [PubMed: 4324897]
45. Beinert H, Shaw RT. Biochim Biophys Acta. 1977; 462:121–130. [PubMed: 199250]
46. Tuckerman JR, Gonzalez G, Sousa EHS, Wan X, Saito JA, Alam M, Gilles-Gonzalez M-A. Biochemistry. 2009; 48:9764–9774. [PubMed: 19764732]
47. Kurokawa H, Lee DS, Watanabe M, Sagami I, Mikami B, Raman CS, Shimizu T. J Biol Chem. 2004; 279:20186–20193. [PubMed: 14982921]
48. Hirata S, Matsui T, Sasakura Y, Sugiyama S, Yoshimura T, Sagami I, Shimizu T. Eur J Biochem. 2003; 270:4771–4779. [PubMed: 14622266]
49. Park H, Suquet C, Satterlee JD, Kang C. Biochemistry. 2004; 43:2738–2746. [PubMed: 15005609]
50. Gonzalez G, Dioum EM, Bertolucci CM, Tomita T, Ikeda-Saito M, Cheesman MR, Watmough NJ, Gillez-Gonzalez M-A. Biochemistry. 2002; 41:8414–8421. [PubMed: 12081490]
51. Ishitsuka Y, Araki Y, Tanaka A, Igarashi J, Ito O, Shimizu T. Biochemistry. 2008; 47:8874–8884. [PubMed: 18672892]
52. Chen J-J, London IM. Trends Biochem Sci. 1995; 20:105–108. [PubMed: 7709427]

53. Ishikawa H, Yun B-G, Takahashi S, Hori H, Matts RL, Ishimori K, Morishima I. J Am Chem Soc. 2002; 124:13696–13697. [PubMed: 12431098]
54. Igarashi J, Murase M, Iizuka A, Pichierri F, Martinkova M, Shimizu T. J Biol Chem. 2008; 283:18782–18791. [PubMed: 18450746]
55. Hirai K, Martinkova M, Igarashi J, Saiful I, Yamauchi S, El-Mashtoly S, Kitagawa T, Shimizu T. J Inorg Biochem. 2007; 101:1172–1179. [PubMed: 17597215]
56. Uma S, Yun B-G, Matts RL. J Biol Chem. 2001; 276:14875–14883. [PubMed: 11278914]
57. Roberts GP, Kerby RL, Youn H, Conrad M. J Inorg Biochem. 2005; 99:280–292. [PubMed: 15598507]
58. Kerby RL, Ludden PW, Roberts GP. J Bacteriol. 1995; 177:2241–2244. [PubMed: 7721719]
59. Reynolds MF, Shelver D, Kerby RL, Parks RB, Roberts GP, Burstyn JN. J Am Chem Soc. 1998; 120:9080–9081.
60. Lanzilotta WN, Schuller DJ, Thorsteinsson MV, Kerby RL, Roberts GP, Poulos TL. Nat Struct Biol. 2000; 7:876–880. [PubMed: 11017196]
61. Shelver D, Torsteinsson MV, Kerby RL, Chung S-Y, Roberts GP. Biochemistry. 1999; 38:2669–2678. [PubMed: 10052937]
62. Aono S, Ohkubo K, Matsuo T, Nakajima H. J Biol Chem. 1998; 273:25757–25764. [PubMed: 9748246]
63. Clark RW, Youn H, Parks RB, Cherney MM, Roberts GP, Burstyn JN. Biochemistry. 2004; 43:14149–14160. [PubMed: 15518565]
64. Kerby RL, Youn H, Thorsteinsson MV, Roberts GP. J Mol Biol. 2003; 325:809–823. [PubMed: 12507482]
65. Youn H, Kerby RL, Roberts GP. J Biol Chem. 2003; 278:2333–2340. [PubMed: 12433917]
66. Yamamoto K, Ishikawa H, Takahashi S, Ishimori K, Morishima I, Nakajima H, Aono S. J Biol Chem. 2001; 276:11473–11476. [PubMed: 11278259]
67. Reynolds MF, Parks RB, Burstyn JN, Shelver D, Thorsteinsson MV, Kerby RL, Roberts GP, Vogel KM, Spiro TG. Biochemistry. 2000; 39:388–396. [PubMed: 10631000]
68. Kitanishi K, Igarashi J, Hayasaka K, Hikage N, Saiful I, Yamauchi S, Uchida T, Ishimori K, Shimizu T. Biochemistry. 2008; 47:6157–6168. [PubMed: 18479150]
69. Tanaka A, Takahashi H, Shimizu T. J Biol Chem. 2007; 282:21301–21307. [PubMed: 17535805]

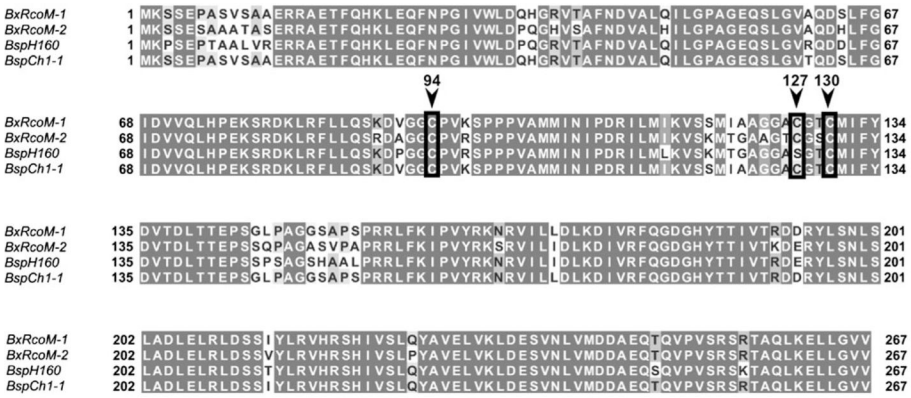

Fig. 1.

Sequence alignments of *Burkholderia xenovorans* regulator of CO metabolism 1 (*BxRcoM-1*; UniProt accession no. Q13YL3; NCBI gi:123168453) and *B. xenovorans* regulator of CO metabolism 2 (*BxRcoM-2*; UniProt accession no. Q13IY4; NCBI gi: 122969446) with two putative RcoM proteins from *Burkholderia cepacia* H160 (*BspH160*; UniProt accession no. B5WBI7) and *B. cepacia* CH1-1 (*BspCh-1*; UniProt accession no. D5NG05). All Cys residues are boxed in *black*; the appropriate numbering is indicated *above an inverted arrow*. The alignments show high amino acid conservation among all sequences, including complete conservation of Cys^{94} and Cys^{130}, but not Cys^{127}

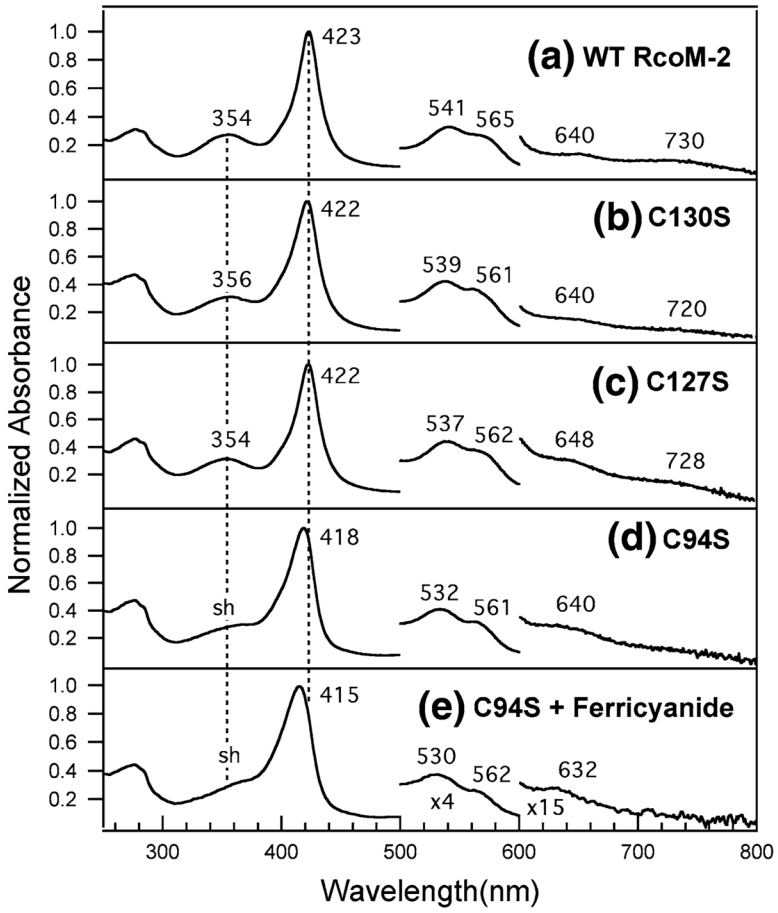

Fig. 2.

Electronic absorption spectra of purified wild-type (*WT*) BxR-coM-2 (*a*), C130S (*b*), C127S (*c*), C94S (*d*), and C94S (*e*) reacted with potassium ferricyanide. Spectra *a*–*d* were taken of the protein as isolated; spectrum *e* was taken after oxidation of the protein with potassium ferricyanide and removal of excess oxidant via a spin concentrator. The sample for spectrum *a* contained 12 μM heme in 25 mM 3-[4-(2-hydroxyethyl)-1-piperazinyl]propanesulfonic acid (EPPS) pH 8.0 with 500 mM KCl; the samples for spectra *b*–*d* contained 8–10 μM heme in 25 mM 3-(*N*-morpholino)propanesulfonic acid (MOPS) pH 7.4 with 500 mM KCl. *sh* shoulder

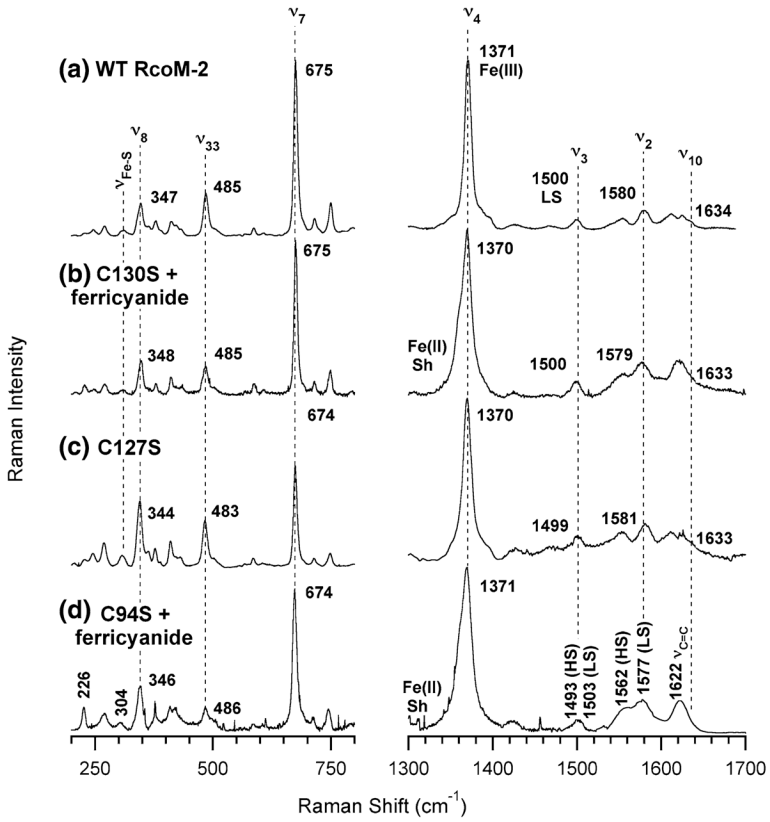

Fig. 3.

Resonance Raman spectra of WT Fe(III)BxRcoM-2 (*a*), C130S reacted with potassium ferricyanide (*b*), C127S (*c*), and C94S reacted with potassium ferricyanide (*d*). The sample for spectrum *a* contained 250 μM heme in 50 mM borate pH 8.0 with 500 mM KCl; the samples for spectra *b*–*d* contained 80–170 μM heme in 25 mM MOPS, pH 7.4, with 500 mM KCl. Spectra were acquired with 8–15-mW of power at the frozen (77 K) sample using the 413.1-nm Kr^+ laser line. Key porphyrin stretching modes are noted, including major oxidation-state and spin-state marker bands (ν_2, ν_3, ν_4, and ν_{10}) and the putative Fe–S stretch band ($\nu_{Fe–S}$)

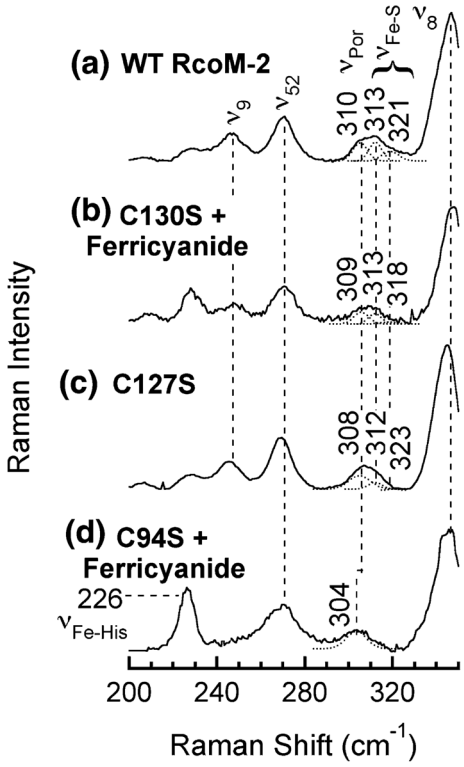

Fig. 4.

Low-frequency resonance Raman spectra of WT Fe(III)BxR-coM-2 (*a*), C130S reacted with potassium ferricyanide (*b*), C127S (*c*), and C94S reacted with potassium ferricyanide (*d*). The sample for spectrum *a* contained 250 μM heme in 50 mM borate, pH 8.0, with 500 mM KCl; the samples for spectra *b*–*d* contained 80–170 μM heme in 25 mM MOPS, pH 7.4, with 500 mM KCl. Spectra were acquired with 8–15 mW of power at the frozen (77 K) sample using the 413.1-nm Kr^+ laser line. Key stretching modes are noted, including the Gaussian deconvolution of the putative Fe–S stretch band, $\nu_{Fe–S}$, the overlapping porphyrin mode, ν_{Por}, and the putative $\nu_{Fe–His}$ stretch. Peak positions are indicated for the putative porphyrin stretching mode ν_{Por} that overlaps with $\nu_{Fe–S}$

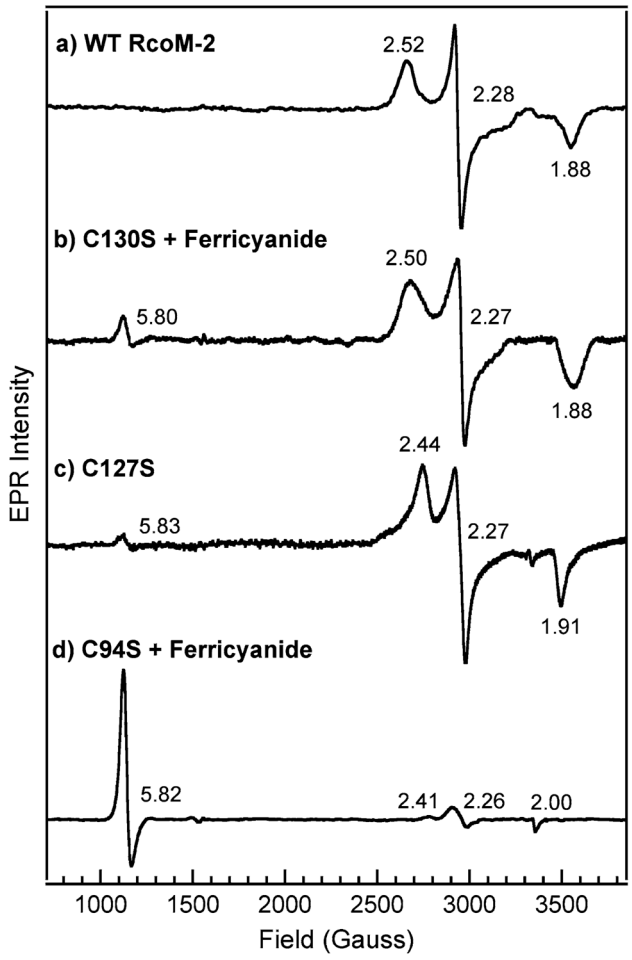

Fig. 5.

X-band electron paramagnetic resonance (*EPR*) spectra of WT Fe(III)BxRcoM-2 (*a*), C130S reacted with ferricyanide (*b*), C127S (*c*), and C94S reacted with ferricyanide (*d*). The sample for spectrum *a* contained 250 μM heme in 50 mM borate, pH 8.0, with 500 mM KCl; the samples for spectra *b*–*d* contained 80–170 μM heme in 25 mM MOPS, pH 7.4, with 500 mM KCl. The spectra were recorded at 10 K, 9.38-GHz microwave frequency, less than 5-mW microwave power, 65-dB receiver gain, 8.00-G modulation amplitude, 100-kHz modulation frequency, and 81.92-ms time constant and used 20 added scans, each containing 2,048 data points, except for spectrum *a*, for which 9.36-GHz microwave frequency, 8.31-G modulation amplitude, and 163.84-ms time constant were used, spectrum *c*, for which 9.36-GHz microwave frequency, 8.31-G modulation amplitude, and ten averaged scans were used, and spectrum *d*, for which10.02-mW microwave power was used

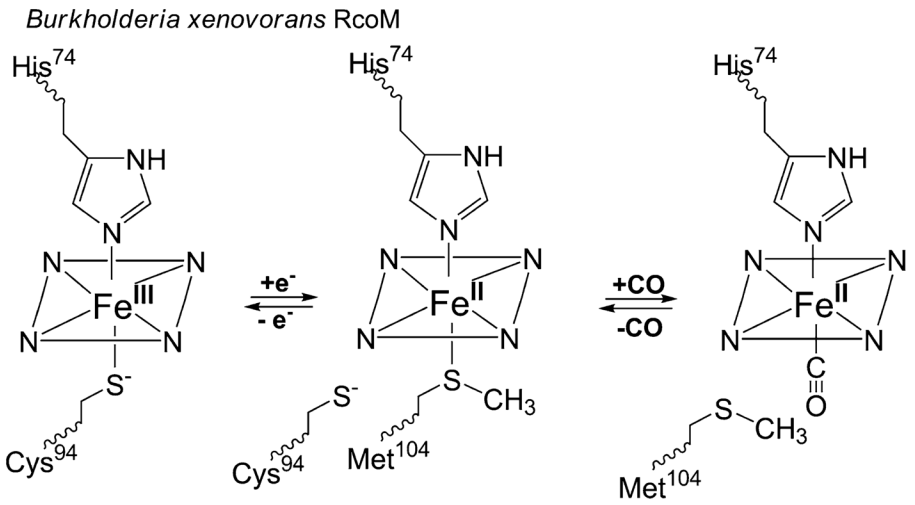

Scheme 1.

The varying heme coordination environments in *Burkholderia xenovorans* regulator of CO metabolism (*RcoM*). Reduction of Fe(III) heme to Fe(II) heme results in loss of the cysteine(thiolate) ligand (Cys^{94}), which is replaced by a nearby methionine (Met^{104}). Introduction of CO results in replacement of the weakly bound Fe(II) distal Met^{104} ligand to form a carbon monoxy adduct. In all states, the proximal ligand is a histidine (His^{74}) that is retained

Table 1

Comparison of electronic absorption peak positions (nm) for the CxxS *Burkholderia xenovorans* regulator of CO metabolism 2 (*BxRcoM-2*) variants with wild-type (*WT*) BxRcoM-2 in the Fe(III), Fe(II), and Fe(II)CO states

	Ligands	δ	Soret	β	α	LMCT	Reference
Fe(III)							
WT BxRcoM-2	Cys/His	354	423	541	565	640, 730	[25]
C130S[a]		356	422	539	561	640, 720	This work
C127S[a]		354	422	537	562	648, 728	This work
C94S[a]		sh	418	532	561	640	This work
C94S + ferricyanide		sh	415	530	562	632	This work
Fe(II)							
WT BxRcoM-2	Met/His		425	532	562		[25]
C130S			425	532	562		This work
C127S			424	532	562		This work
C94S			425	532	562		This work
C94S + ferricyanide			426	531	562		This work
Fe(II)CO							
WT BxRcoM-2	His/CO		423	540	570		[25]
C130S			423	540	569		This work
C127S			423	539	568		This work
C94S			423	540	570		This work
C94S + ferricyanide			423	540	570		This work

LMCT ligand-to-metal charge transfer, *sh* shoulder

[a]These data are provided for the protein as isolated; the sample may contain a fraction of the Fe(II) form

J Biol Inorg Chem. Author manuscript; available in PMC 2012 October 31.

Table 2

Comparison of electron paramagnetic resonance *g* values for the CxxS BxRcoM-2 variants and those of WT BxRcoM-2

Protein	Ligands	g_z	g_y	g_x	pH	Reference
WT BxRcoM-2	His/Cys	2.52	2.28	1.88	8.0	[25]
C130S[a] BxRcoM-2		2.50	2.28	1.87	7.4	This work
C127S BxRcoM-2		2.44	2.27	1.91	7.4	This work

Protein	$g_\perp$	$g_\parallel$	pH	Reference
C94S[a] BxRcoM-2	5.82	2.00	7.4	This work

[a]The spectrum was obtained after reaction of the as-isolated protein with ferricyanide